Applied Catalysis B: Environmental 258 (2019) 118016

Contents lists available at ScienceDirect

Applied Catalysis B: Environmental

journal homepage: www.elsevier.com/locate/apcatb

Electron-poor copper nanoparticles over amorphous zirconia-silica as *all-in-one* catalytic sites for the methanol steam reforming

Filippo Bossola[a], Nicola Scotti[a], Ferenc Somodi[b], Mauro Coduri[c,d], Claudio Evangelisti[a], Vladimiro Dal Santo[a,*]

[a] CNR—Istituto di Scienze e Tecnologie Molecolari, Via C. Golgi 19, 20133 Milano, Italy
[b] Centre for Energy Research, Konkoly-Thege M. street 29-33, H-1121 Budapest, Hungary
[c] ESRF – The European Synchrotron, 71, avenue des Martyrs, 38000, Grenoble, France
[d] Currently at Department of Chemistry, University of Pavia, Viale Taramelli 16, 27100 Pavia, Italy

ARTICLE INFO

Keywords:
Zirconia-silica
Copper nanoparticles
Methanol steam reforming
Synchrotron-XRPD
XPS

ABSTRACT

The addition of a specific amount of silica (10 wt.%) to zirconia was found to significantly influence the morphological and electronic properties of supported copper nanoparticles in a Cu/ZrO_2-SiO_2 catalyst. The so-developed catalyst was tested in the methanol steam reforming reaction and reached at 3500 h^{-1} of space velocity a hydrogen productivity of 370 mmol h^{-1} $g_{cat}{}^{-1}$, that is four times higher than that obtained with a Cu/ZrO_2 catalyst. The reason of such an improved activity was elucidated via a series of *in-situ* characterization, including synchrotron XRPD, XPS, and FTIR analyses with probe molecules. The results show that the addition of silica inhibits both the crystallization of the support and the copper reduction, leading to particularly small and stable copper nanoparticles ranging 2–3 nm in diameter. Although completely reduced and in the metallic state (neither Cu^{2+} nor Cu^{+} were detected), these so-small nanoparticles feature a markedly electron poor surface on which methanol preferentially adsorbs. Since both the dehydrogenation of the intermediates and the subsequent molecular hydrogen formation are performed by the same site, the hydrogen production rate results markedly boosted. The drawback of having a different adsorption site and two distinct Cu^0 and Cu^{+} sites is thus overcome thanks to this *all-in-one* catalytic site, and the copper actually participating to all the reaction is maximized.

1. Introduction

The introduction of unsaturated sites is proving quite effective in promoting reforming reactions with simple substrates, such as methane, methanol and ethanol [1–4], or molecules bearing only alcoholic functionalities, such as glycerol and xylitol [5–8]. And much work is being devoted trying to elucidate the actual promoting mechanisms [1,5,6].

For instance, Llorca and co-workers [2] recently discovered that the outstanding stability of the Co/Hydrotalcite catalysts under ethanol steam reforming conditions is due to the incomplete reduction of the cobalt sites which strongly inhibits the formation of carbon deposits.

Other examples are the works on glycerol reforming by Wang and co-workers [5–7] on the addition to platinum of promoters in the form of a less reducible metal (like manganese [5]), or one that partially oxidizes under working conditions (like rhenium [6,7]). Such promoters basically act as Lewis acid centers thereby enhancing the initial dehydrogenation step of the reforming reaction [6].

One of the most emblematic cases that is still being studied due to its high versatility and only apparent simple nature is the Cu/ZrO_2 catalyst. It is active in the alcohols upgrading [9] and methanol synthesis [10,11], and to produce hydrogen via water gas shift reaction [12], methanol decomposition [13–15], and methanol steam reforming (MSR) [1,16–20].

Two factors mostly affect the reactivity of Cu/ZrO_2 catalysts, namely the coexistence of metallic copper and Cu^{+} sites under reaction conditions and the exposed copper phase [1,21–25]. Seen from the MSR point of view, metallic copper is the responsible for the molecular hydrogen evolution from the atomic hydrogen which in turn is extracted from the intermediates by the Cu^{+} sites [26]. In addition to this dehydrogenative role, Cu^{+} sites are important for the conversion of CO to CO_2 that must be maximized in order to obtain near-CO free hydrogen streams [27].

But the coexistence of these two species, although necessary, represents a limit. Such splitting in the roles implies that no copper participates to all the reaction steps, therefore quite high copper

* Corresponding author.
E-mail address: vladimiro.dalsanto@cnr.it (V. Dal Santo).

https://doi.org/10.1016/j.apcatb.2019.118016
Received 14 March 2019; Received in revised form 23 July 2019; Accepted 27 July 2019
Available online 30 July 2019

loadings are necessary to achieve reasonable hydrogen productivities [18,20].

The most common strategy adopted to cope with this limitation is having a copper dispersion as high as possible, and so co-precipitation methods are widely employed for the catalysts preparation [1,18,20,28–32]. The only problem with this approach is that upon calcination copper migrates to the surface of the catalysts and agglomerates compromising the catalytic performances [33]. The calcination is required in order to stabilize the amorphous zirconia and prevent undesired phase transitions during the reaction [33], and to incorporate some of the copper into the lattice of the support so that Cu^+ sites may form [11,34].

The use of incipient wetness technique was (re)conjured by Tada et al. [10] as viable means to increase the contact between metallic copper and Cu^+ sites without losing too much copper into the support lattice. Contrary to many previous works [1,19,21,35], they reported as best support the amorphous zirconia since it led to a higher copper dispersion than with the other polymorphs. Nonetheless, this solution does not overcome the problem of having two distinct catalytic sites with two distinct roles.

It is known that copper deposited on zirconia reduces more easily than copper deposited on other oxides, like silica [9,36]. For instance, this poor interaction of copper with silica was exploited by Yang et al. [26] to produce copper nanoparticles particularly rich in Cu^+ sites which allowed the authors to elucidate their role in the reactivity with methanol. The difference in reducibility means that by changing the support it is possible to modulate the electronic properties of the copper nanoparticle.

A good example of exploiting such effect is the previously cited work by Llorca and co-workers [2]. They used different polymorphs of a Mg-Al mixed oxide to tune the final electronic state of the active metal. The cobalt deposited on the spinel phase was totally reduced, whereas on hydrotalcite only a partial reduction was observed. The so electron-poor cobalt sites are active in the steam reforming of ethanol but lack the necessary electron density to promote the formation of filamentous carbon thus dramatically lengthening the catalyst life.

In the work by Tada et al. [10] the authors observed that, unlike a Cu/ZrO_2 catalyst, treating with hydrogen at 350 °C a $Cu/ZrO_2/SiO_2$ catalyst, only the 12% of copper is reduced to Cu^0, while the rest is composed of Cu_2O and CuO. The persistence of unreduced copper after the reduction treatment demonstrates that silica might have a direct influence on the copper phase and its electronic properties, even when it is used just as support.

It is interesting to note that in many of the research works on zirconia-supported copper nanoparticles the influence of the silica is often poorly considered or not stressed enough. It is widely known, especially by the users of silica-based chromatographic columns [37], that silica dissolves at high pH values [38]. Because most of the synthetic procedures reported in the literature involve the use of basic solutions and often the description of the equipment is not detailed, involuntary silica contaminations might occur if carried out in classical lab glassware. Moreover, besides altering the copper reduction, silica is reported to retard the crystallization of zirconia [39], so its presence might impact the overall catalyst.

Furthermore, zirconia and silica interact differently with methanol, as evidenced by Bell and co-workers [13,40–42] and others [31,43,44]. They reported that methanol practically does not adsorb on silica, while on Cu/ZrO_2 it adsorbs preferentially on the zirconia support. Their investigations thus suggest that methanol adsorption might be controlled, or at least preferentially directed, by finding the optimum catalyst composition and morphology.

The MSR reaction is among those promising processes that might be playing a pivotal role in the future hydrogen economy, especially for hydrogen-fueled vehicles [45]. Cu/ZrO_2 catalysts generally offer improved performances and high CO_2 selectivity when compared to other systems [1,39]. Much work is being carried out, mainly with the double aim of reducing the copper content, which often is more than the 40–50 wt.% of the catalyst [18,20,32,46,47], and retarding the copper agglomeration. Dopants such as ceria or yttria [1,29,30] are typically added to the catalysts to promote the CO oxidation [29] and/or to increase the fraction of Cu^+ sites [30,48] whereas zinc oxide promotes copper dispersion and stability [46,49]. But in none of these works the presence of Cu^+ sites was considered as an obstacle to the improvement of the catalytic activity.

So, in order to overcome such limitation imposed by the coexistence of well-defined Cu^0 and Cu^+ sites, we present in this work an innovative approach to improve the catalytic performances of a Cu/ZrO_2 catalyst by developing an *all-in-one* active site for the hydrogen production. Via a series of *in-situ* characterizations, including synchrotron XRPD, XPS and FTIR with probe molecules, we show how the modulation of the composition of a zirconia-silica support dramatically impacts the copper nanoparticles formation, their final electronic properties and the surface chemistry of the catalyst, and how all this can be exploited to greatly propel the hydrogen productivity in the MSR reaction.

2. Experimental

2.1. Catalyst preparation

The zirconia-silica supports were prepared by a sol-gel procedure. First, a zirconyl chloride ($ZrOCl_2$) solution 30% in HCl (Sigma-Aldrich) (13 mL) was diluted to 100 mL with deionized water; such solution was then added dropwise at room temperature to 200 mL of an aqueous solution of ammonia at pH of 12 to obtain a hydrous zirconia. A solution of tetraethylorthosilicate (Sigma-Aldrich):2-propanol:water (1:6:2 mole ratio, respectively) was added to the hydrous zirconia and the suspension was vigorously stirred for 3 days at 75 °C. The so-obtained solid was thoroughly washed with deionized water until pH neutrality, followed by drying overnight at 110 °C in air. Finally, the solid was calcined at 350 °C for 4 h in air. Five supports were prepared with different amounts of silica (0, 3, 10, 15, and 30 wt.%). In order to avoid any silicon contamination from the glass containers, a Teflon container was used to prepare the pure zirconia support. Copper (15 wt.%) was deposited by incipient wetness impregnation technique using copper nitrate trihydrate ($Cu(NO_3)_2{\cdot}3H_2O$) (Sigma-Aldrich) as precursor, followed by calcination in air at 350 °C for 4 h. The catalysts were labelled as Cu/ZrSiX, with X being the nominal amount of silica in the support. The catalyst containing no silica was labelled as Cu/Zr.

2.2. Catalyst characterization

BET surface area, BJH pore volume, and pore size distribution were measured by a Micromeritics ASAP2020 using nitrogen as adsorptive gas at −196 °C. The samples were outgassed at 130 °C for 4 h prior to the analyses.

Copper loadings were determined by inductively coupled plasma–optical emission spectrometry (ICP–OES) (ICAP 6300 Duo, Thermo Fisher Scientific) after digestion in *aqua regia*.

Hydrogen temperature programmed reduction (H_2-TPR) experiments were performed with a Micromeritics PulseChemisorb 2700. The samples were treated at 110 °C for 1 h under Ar flow (30 mL min^{-1}). The temperature was then ramped up at 8 °C min^{-1} to 550 °C under 8 vol.% H_2/Ar flow at 10 mL min^{-1}.

Copper dispersion was calculated by using the same apparatus of the H_2-TPR experiments. The samples were first reduced by flowing 8 vol.% H_2/Ar and increasing the temperature to 270 °C at a rate of 8 °C min^{-1} and held for 1 min, followed by cooling to 70 °C under Ar flow at 30 mL min^{-1}. The so-reduced samples were then treated with a N_2O/Ar flow (60 mL min^{-1}) for 5 min, after which the reduction procedure was repeated.

Copper dispersion was calculated according the following equation

[50,51]:

$$D_{Cu} = \frac{2\,A_2}{A_1}\,100$$

Here, the terms are as follows: D_{Cu} is the copper dispersion (%), A_1 and A_2 are the integrated areas of the reduction profiles prior and after the treatment with N_2O, respectively.

Exposed surface copper was calculated using the following equation:

$$S_{Cu} = \frac{2\,A_1\,N_A}{100(A_2)(AM_{Cu})(1.4*10^{19})}\,Cu_{tot}$$

Here, the terms are as follows: S_{Cu} is the exposed surface copper ($m_{Cu}^2\ g_{cat}^{-1}$), N_A is the Avogadro number (atoms mol^{-1}), AM_{Cu} is the atomic mass (g mol^{-1}), $1.4 * 10^{19}$ is the surface copper packing density (atoms m^{-2}), and Cu_{tot} is the copper loading (% mass).

Fast Fourier infrared spectroscopy (FT-IR) experiments were performed using a Biorad FTS-60A instrument with methanol and pyridine as probe molecules. The procedure for the methanol desorption experiments is the following. The samples were pressed in 13 mm self-supporting pellets, transferred to the IR cell, and then reduced in hydrogen atmosphere at 300 °C for 30 min. After cooling to room temperature in high vacuum and collecting a spectrum, the samples were contacted with water vapors at 260 °C for 10 min. The samples were then evacuated for 30 min in high vacuum at room temperature to eliminate the excess of water. The very same procedure was adopted with methanol, with the only difference that the adsorption step was carried out at room temperature. The methanol desorption was performed stepwise by heating-up the IR cell in high vacuum at 100, 150, 200, 260, and 300 °C for 30 min. A spectrum was collected for each temperature using as background the spectrum of the sample after the adsorption of water. In the experiments with pyridine, the procedure was the same with the exception that no water was adsorbed before contacting the probe with the sample.

X-ray powder diffraction (XRPD) data were collected at the High Resolution Powder Diffraction beamline (ID22) of the European Synchrotron Radiation Facility (ESRF), Grenoble, France, with incident radiation wavelength 0.45107 Å (~27.5 keV). Amorphous quantification was performed mixing the original powders with 10% by weight of Al_2O_3 NIST as internal standard, using kapton capillaries 0.7 mm in diameter. Three to five batches were prepared for each composition for reproducibility. Data were collected with the high resolution setup of the beamline to account for the narrow profile of the standard and for accurate determination of lattice parameters and intensities. Each acquisition lasted about 2 h. The amorphous fraction X_{am} was estimated after:

$$X_{am} = 1 - \left(\frac{w_{std}}{w_{samp}}\right)\left(\frac{1}{w_{stdR}} - 1\right)$$

where w_{std} and w_{samp} are the relative weight fractions of standard and samples, respectively, and w_{stdR} is the weight fraction of the standard returned by the Rietveld refinement.

In-situ investigations were performed filling the powders into quartz capillaries 0.5 mm in diameter. The capillary, open on one side, was connected to the gas rig available at the ID22 beamline [52] and mounted on a rotating stage. After pumping the sample section, 7 bar of H_2 (10 vol.% diluted in He) were dosed to the sample. The procedure was repeated three times. Then, the capillary was heated up with a hot air blower up to 270 °C at 10 °C min^{-1} and the temperature was held for one hour. Then the hot air blower was removed and a final pattern was collected at room temperature. The pressure of the diluted gas dosed to the sample was chosen after some tests to guarantee at the same the reduction of the catalysts in the same conditions, still avoiding a too fast reduction that could conceal possible intermediate phases.

A Perkin Elmer 2D detector was used for rapid acquisition of XRPD patters. The detector was placed orthogonal to the beam at 1.4 m distance from the sample to guarantee good resolution and a significant amount of Bragg peaks. The sample to detector distance was calibrated against a LaB6 660c NIST standard. Integration of 2D images into full patterns was performed using pyFAI [53]. Phases were identified using QualX [54], while GSAS [55] was used for their quantification as well as for determination of lattice parameters through Rietveld refinements.

Transmission electron microscopy (TEM) analyses were carried out with a ZEISS LIBRA200FE microscope equipped with a 200 kV FEG source. Energy-dispersive X-ray spectroscopy (EDS – Oxford INCA Energy TEM 200) and elemental mapping were collected along with HAADF-STEM (high angular annular dark field scanning electron microscopy) images. The specimens were finely smashed in an agate mortar, suspended in isopropanol and sonicated, then each suspension was dropped onto a holey carbon coated molybdenum grid (300 mesh) letting the solvent evaporate.

For the determination of surface composition and oxidation state of copper, X-ray photoelectron spectroscopy (XPS) measurements were done using a KRATOS XSAM 800 XPS machine equipped with an atmospheric pretreatment chamber. Al Ka characteristic X-ray line, 40 eV pass energy and FAT mode were applied for recording the XPS lines of Cu 2p, Cu LMM, O 1s, Zr 3d, C 1s, Si 2p regions. Si 2p binding energy at 103.3 eV was used as reference for charge compensation in the case of silica containing samples, while Zr $3d_{5/2}$ was used in the case of Cu/Zr catalyst. The samples were measured as synthesized and after reduction in H_2 at 270 °C for 30 min in the atmospheric pretreatment chamber of the spectrometer. Atmospheric pretreatment chamber connected to the UHV chamber with a load lock gate allowed us to do pretreatments without contacting the sample with air.

2.3. Catalytic experiments

The catalytic measurements were carried out with a home-made test unit described in our previous work [56]. A fixed-bed quartz reactor (9 mm internal diameter) was used with catalyst loadings of 200 mg (45-35 mesh). Prior to the catalytic runs, the catalysts were reduced at 270 °C under H_2 flow (15 mL min^{-1}) for 1 h. The reactions were performed at 260 °C by feeding a methanol/water solution with a steam-to-carbon (S/C) molar ratio of 1.3 at 0.03 mL min^{-1}. The Gas Hourly Space Velocity (GHSV), calculated as the volumetric flow rate of the inlet gas divided by the catalyst bed density, was about 3500 h^{-1} for all the catalytic runs. The gaseous products were analyzed with an on-line GC-TCD (Agilent 6890 N).

Conversion was calculated using the following equation:

$$X = \left(1 - \frac{F_{out}}{F_{in}}\right)100$$

Here, the terms are as follows: conversion is X, methanol feed rate is F_{in}, and F_{out} is the reaction products flow rate detected with the GC.

Selectivity was calculated on a carbon base, according to the following equation:

$$Sel_i = \left(\frac{C_i\,F_i}{\sum C_i\,F_i}\right)100$$

Here, the terms are as follows: Sel_i is the selectivity to a product compound, for example CO_2, C_i is the number of carbon atoms in the product compound, and F_i is the molar flow rate of the product.

Hydrogen production rate is expressed as millimoles of hydrogen per hour per gram of catalyst (mmol $h^{-1}\ g_{cat}^{-1}$) or as otherwise stated. The turnover frequencies (TOF) were calculated as rate of carbon moles converted, as mmol $s^{-1}\ kg_{cat}^{-1}$, over the copper dispersion.

Table 1
Physiochemical characterization of the catalysts.

Entry	BET surface area ($m^2 g^{-1}$)	Pore volume ($cm^3 g^{-1}$)	Cu loading (wt. %)
Zr	222	0.37	–
ZrSi3	281	0.34	–
ZrSi10	309	0.34	–
ZrSi15	346	0.42	–
ZrSi30	353	0.60	–
Cu/Zr	141	0.25	12.8
Cu/ZrSi3	184	0.26	14.7
Cu/ZrSi10	216	0.25	13.7
Cu/ZrSi15	181	0.21	13.0
Cu/ZrSi30	205	0.45	12.2

3. Results and discussion

In Table 1 are summarized the morphological properties of the supports and the catalysts. The nitrogen adsorption isotherms and the pore size distributions are reported in Figures S1 and S2.

The pure zirconia features a specific surface area of 222 $m^2 g^{-1}$ and a pore volume of 0.37 $cm^3 g^{-1}$, which are in line with the values reported for zirconia prepared by comparable methods [39]. With the addition of silica, the surface area increases up to 353 $m^2 g^{-1}$ in the ZrSi30 support, but not linearly. In fact, both the samples ZrSi3 and ZrSi10 gain about 60-70 $m^2 g^{-1}$ over the pure zirconia, while the samples ZrSi15 and ZrSi30 gain additional 30-40 $m^2 g^{-1}$. The very same trend can be observed in the pore volumes. With the addition of copper via incipient wetness impregnation technique, both the surface area and the pore volume of the materials decrease, but again a distinction can be observed between the pairs ZrSi3 - ZrSi10 and ZrSi15 - ZrSi30. The former shows a decrease of about 93-97 $m^2 g^{-1}$ while the latter of 165-148 $m^2 g^{-1}$.

According to this first morphological characterization, the silica-containing catalysts can be divided in two groups. For low levels of silica, i.e, 3 and 10 wt.%, the morphological properties resemble those of the pure zirconia, whereas for higher levels, i.e., 15 and 30 wt.%, they change significantly.

The copper dispersion and the exposed surface area of the Cu/Zr, Cu/ZrSi10, and Cu/ZrSi30 catalysts were determined by N_2O titration. These samples were specifically selected as representative of the pure zirconia support and of the two pairs previously identified on the basis of the morphological features. The values are listed in Table 2 along with the crystal sizes found by XRPD and HRTEM. Interestingly, the copper dispersion is fairly high in all the catalysts, with Cu/Zr and Cu/ZrSi30 showing 44.0% and 48.1%, respectively, while Cu/ZrSi10 stands out for its remarkable 60.9%. Assuming cubo-octahedron shaped copper nanoparticles [50,51], these dispersions correspond to nanoparticles sizes in the order of 4–5 nm and 6–7 for the Cu/Zr and Cu/ZrSi30 catalysts, respectively, and of about 2–3 nm for Cu/ZrSi10.

Despite the poor contrast of the HRTEM micrographs [58], such small nanoparticles can be observed in the Cu/ZrSi10 (Fig. 1A), as well as in the Cu/Zr and Cu/ZrSi30 catalysts (Figures S3 and S4). The nanoparticles distributions are reported in Figure S5. The mean copper nanoparticles sizes in Cu/Zr and Cu/ZrSi30 catalysts are quite similar and centered at 4.3 nm and 4.6 nm, respectively. In line with the values determined by N_2O titration, the copper nanoparticles in Cu/ZrSi10 are smaller (3.1 nm mean size) and with a narrower distribution (Figure S5). The same trend among the particles sizes of the three samples was observed also by synchrotron-radiation XRPD analyses (Table 2).

So small copper nanoparticles supported on zirconia have never been reported in the literature for reforming applications [1,21], and the typical sizes are in the order of tenths of nanometers even on ZnO [1,59]. Only for silica support and for other reactions, copper nanoparticles as small as 3 nm were reported [50,60].

HAADF-STEM/EDX maps of the samples revealed no segregation of both zirconium and silicon in the support grains together with a homogeneous dispersion of copper (Fig. 1B-E and Figures S6 and S7). In the Cu/Zr catalyst, the surface composition of the supports is, as expected, pure zirconia. In Cu/ZrSi10 and Cu/ZrSi30 the Zr/Si molar ratios, as detected by EDX analyses, resulted about 4 and 1, respectively, in line with the nominal amounts used for the synthesis. These ratios were confirmed by the XPS analyses (Table S3) proving the high compositional homogeneity of the prepared ZrSiX supports.

Some other insights on the structure of the supports can be deduced from the HRTEM. In both the samples containing silica (Fig. 1 and Figure S4), no crystalline zirconia was observed, but rather the supports appeared to be totally amorphous. The absence of crystallinity is expected [39] and explains the high surface are of these samples.

Another peculiarity observed in all the samples (Fig. 1 and Figures S3, S4, S6, and S7), but more evidently in those containing silica, is that the copper nanoparticles appear to be always well-included into the support. As already stated, the interaction of copper with the amorphous zirconia is well documented [33] and sometimes results in a loss of available copper with the formation of mixed $Cu_xZr_yO_z$ phases [10,37] and/or the transition to crystalline zirconia [11,34]. But here, in light of the high copper dispersions values and the absence of crystalline zirconia, it might have actually helped in stabilizing the nanoparticles thereby improving the copper-support interface. The precise nature of this interaction and its effect on the copper reducibility will be elucidated with the help of H_2-TPR, *in-situ* XRPD and XPS analyses.

Synchrotron XRPD experimental patterns are reported in Figure S8 and S9, respectively before and after the reduction, while the crystalline phase compositions are reported in Table S1.

Before the reduction, the copper is fully oxidized in the as prepared samples, except for a minor amount of metallic copper detected in the Cu/Zr catalyst.

Two crystalline zirconia phases (tetragonal, space group $P4_2/nmc$, and monoclinic, space group $P2_1/c$) were observed in the sample free of silica (Table S1); in the presence of silica, and irrespective of the content, the supports are totally amorphous.

Details about the data processing together with results for each batch are reported in the SI and in Table S2. The bumps in the background, not consistent with the capillary contribution, suggest important fraction of amorphous. Indeed, the amorphous content increases from 71(3) wt.% in absence of silica, up to 96(1) and 97(1) wt.% by increasing the amount of silica to 10 and 30 wt.%, respectively (Table S2).

These data are quite interesting because although the Cu/Zr catalyst

Table 2
Cu crystalline size, dispersion, and exposed surface area.

Entry	Cu crystallite size[a] (nm)	Cu crystallite size[b] (nm)	Cu crystallite size[c] (nm)	Cu dispersion[b] (%)	Cu surface area[b] ($m^2 g_{cat}^{-1}$)
Cu/Zr	–	4-5	4.3	44.0	38.1
Cu/ZrSi10	5	2-3	3.1	60.9	60.6
Cu/ZrSi30	9	6-7	4.6	41.1	32.7

[a] Cu crystallite size calculated using XRPD by the Williamson-Hall method [57].
[b] Cu crystallite size, dispersion, and exposed surface area calculated by N_2O titration.
[c] Cu crystallite size calculated using HRTEM.

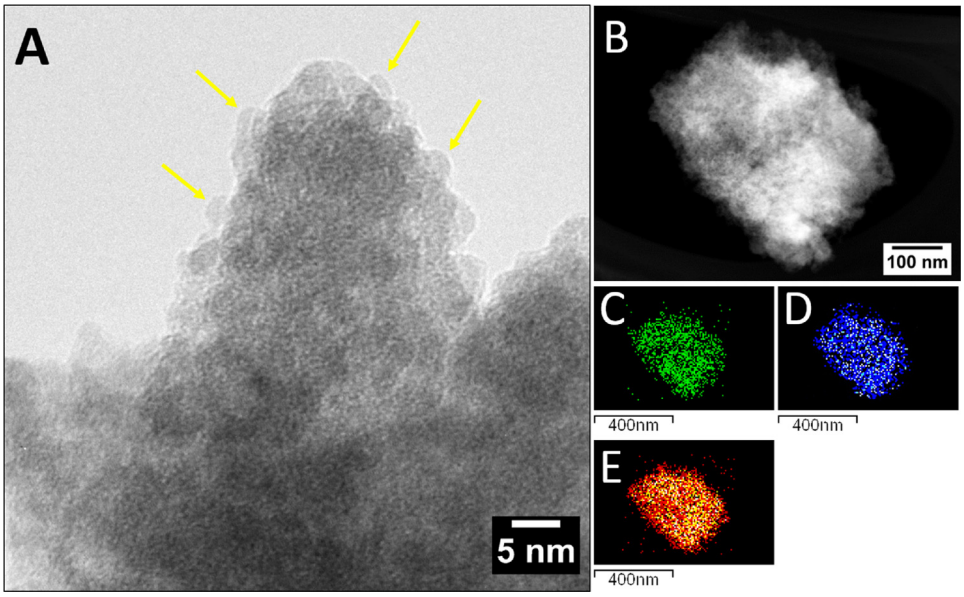

Fig. 1. Representative HRTEM micrograph of Cu/ZrSi10 catalyst (A) and STEM measurements: HAADF image of a catalyst grain (B); STEM-EDX mapping of the catalyst showing the Cu, Si, and Zr dispersions in the catalyst (C–E).

never experienced temperature higher than 350 °C, neither during the catalysts preparation nor during the activation treatment before the reactions, about the 30 wt.% of the support is actually crystalline. However, in some works [11,28], pure zirconia supports prepared in a similar way are reported as almost totally amorphous. This corroborates our suppositions on silica having a major influence on the morphological features.

The evolution of the copper phases during the reduction treatment is reported in Fig. 2. The patterns were collected by heating up the samples to 270 °C and by holding the temperature for 1 h or until complete copper reduction to Cu^0. Table S2 provides the phase composition after 1 h at 270 °C.

In the absence of silica, CuO reduces to metallic copper already upon heating. Full reduction of copper is observed within 20 min, while the zirconia phases are not affected. No intermediate phases were observed. Moreover, the molar fraction of copper-based crystalline phase is not changed upon reduction (˜13%). This suggests that no further crystallization occurs during the treatment.

Conversely, the reduction in catalysts containing silica is accompanied by the formation of intermediate Cu_2O. After 20 min, 85% of copper is reduced in the sample Cu/ZrSi30, while for Cu/ZrSi10 only 60% of copper is reduced, and also some Cu_2O is present. It turns out, then, that the presence of silica slows down the reduction, especially in the catalyst with intermediate content of silica.

Figure S9 shows XRPD patterns collected at room temperature after the *in-situ* investigation, still under reducing atmosphere. The catalysts are fully reduced and only 5 wt.% of residual CuO is observed in Cu/ZrSi30. The Bragg peaks of copper have a peculiar shape, characterized by a broad tail and a narrow top part. The patterns were consequently modeled considering a bimodal distribution, i.e., very small nanoparticles responsible for the broad tail and bigger crystallites leading to sharp character. As an example, the refinement of the pattern for sample Cu/ZrSi10 is reported in the SI with the contribution of the two populations. The fit for the (200) reflection of Cu is shown in Figure S10. This corresponds to 82% of nanoparticles being of about 5 nm in size, as estimated by Williamson-Hall method using 5 reflections [57].

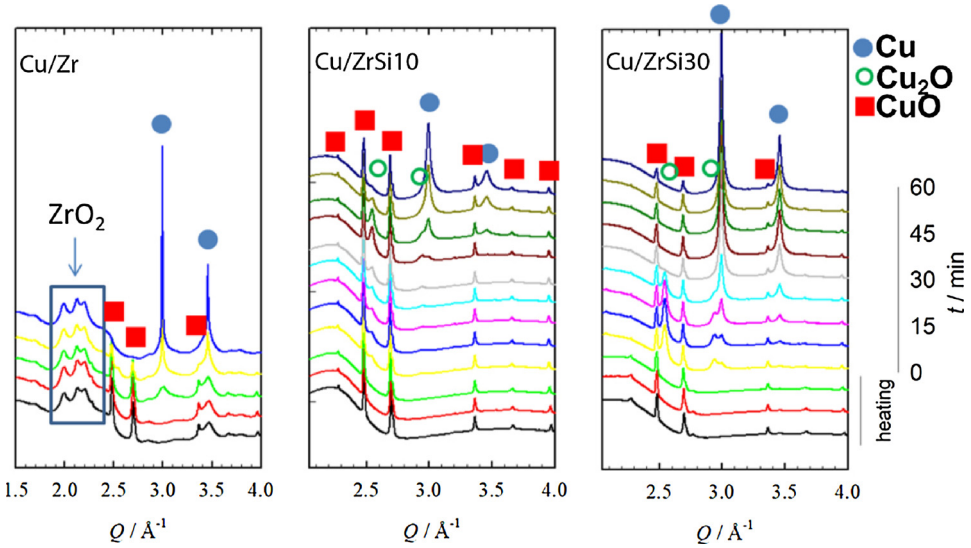

Fig. 2. Phase evolution upon heating from room temperature to 260 °C and while holding temperature per Cu/Zr, Cu/ZrSi10, and Cu/ZrSi30 up to 1 h holding time or till full reduction from CuO to Cu^0. Curves with same colour indicate the same duration of the treatment.

Just as calculated with the N_2O and found with the HRTEM, the nanoparticles in Cu/ZrS30 are bigger with 88% of them being of 9 nm. Unfortunately, it was not possible to determine a size via XRPD for the Cu/Zr catalyst as the peak baseline is too disturbed by contribution of signals from the crystalline zirconia. The size of the larger crystals is hard to determine reliably, as the instrumental contribution to peak broadening is not negligible. It can be estimated in the order of some tens of nanometers. Moreover, copper nanoparticles are known to easily form stacking faults, which may alter significantly the shape of diffraction peaks, therefore affecting the size identification [61].

Among the factors that have contributed to the high dispersion of copper, the high surface of the three supports certainly plays a crucial role. For instance, a similar dispersion was reported by Deshmane et al. [62] for a Cu-MCM-41 catalyst at 14 wt.% copper loading. Supports with lower surface areas were reported as well, but the resulting dispersions are typically in the range of 10–20% [1,30]. However, the surface area of the ordered silica support used by Deshmane et al. [62] is sensitively higher than those of the catalysts herein studied (662 vs. 216 $m^2 g^{-1}$ of Cu/ZrSi10). This means that other factors have contributed to achieving such good copper dispersions, also considering the higher surface area of Cu/ZrSi30 with respect to Cu/ZrSi10.

The reduction of copper is in fact size dependent and autocatalytic [63]. The formation of Cu_2O might have hindered the formation of excessive metallic copper which in turn was stabilized by the zirconia during the reduction treatment thus resulting in very small nanoparticles [36,58,64]. When the support is more enriched in silica, that is in Cu/ZrSi30, such stabilizing effect is lost and the copper nanoparticles are more free to grow.

These data demonstrate that besides on the support itself, silica impacts also the formation of the copper nanoparticles and their final size.

H_2-TPR experiments were performed to better understand the actual reduction profiles and the results are shown in Fig. 3.

The catalyst supported on pure zirconia shows two reduction peaks at 176 °C and 220 °C. The precise assignation of the reduction profiles to specific copper species is not trivial as their position can vary depending on many parameters, such as the crystalline phase of the zirconia [65], the degree of dispersion of the copper [66] and the strength of the metal-support interaction [67]. For sure in the Cu/Zr catalyst a mechanism involving the formation of Cu^+ before the complete reduction to the metallic state [63] can be excluded because no Cu_2O phase was never observed during the in-situ XRPD analyses (Fig. 2).

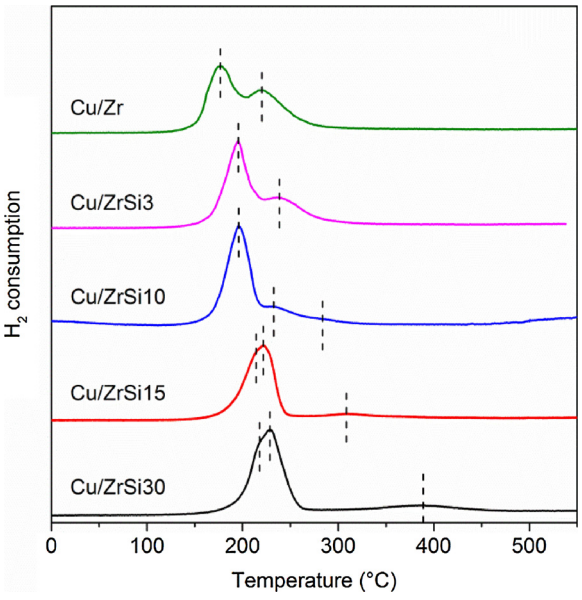

Fig. 3. H_2-TPR analyses of the catalysts.

The presence in this catalyst of both monoclinic and tetragonal zirconia and the high copper dispersion suggest that the two peaks are due to finely dispersed copper nanoparticles deposited onto these two zirconia polymorphs.

Anyhow, with the addition of silica into the support, the high-reduction peak progressively disappears and the main peak shifts to higher temperatures, reaching 230 °C in Cu/ZrSi30. Here again, a distinction between pairs of catalysts can be made based on the shape of the reduction profiles. Specifically, the profiles of Cu/ZrSi3 and Cu/ZrSi10 are very similar, with the main reduction peak centered at 197 °C, while both Cu/ZrSi15 and Cu/ZrSi30 show a reduction feature between 217 °C and 230 °C. This shift can be ascribable to copper nanoparticles progressively losing interaction with the zirconia support due to the increasing content of silica, in line with the reports by Kundakovich and Flytzani-Stephanopoulos [68] and some of us [9].

Some considerations can be drawn based on the characterization data collected so far. The addition of silica does influence the copper nanoparticles by acting on their size and reducibility. More specifically, the catalysts with silica levels below the 10 wt.% display a reducibility similar to copper supported on pure zirconia, whereas at high silica contents the profiles resemble more those typical of copper on silica. Moreover, in Cu/ZrSi10, due to a different reduction path, the copper dispersion results increased and so does the portion of copper available for the reaction. This situation changes dramatically for higher amounts of silica and the catalysts feature harder-to-reduce, bigger copper nanoparticles weakly interacting with a support.

The catalytic runs were performed at 260 °C by feeding a water/methanol solution (S/C molar ratio of 1.3) at a GHSV of 3500 h^{-1}. The results are reported in Fig. 4A as hydrogen productivity per gram of catalyst and methanol conversion after 20 h time-on-stream. A long term stability test was performed only with Cu/ZrSi10 for 100 h (Fig. 4B). In Table 3 are listed also the TOF and the apparent activation energies (E_a).

No methane was detected at these experimental conditions and the carbon monoxide selectivity was always below 0.1%. The bare supports did not display any activity (thus not shown).

The Cu/Zr catalyst reached a methanol conversion of about 20% and a hydrogen production rate of 91 mmol h^{-1} $g_{cat}{}^{-1}$ corresponding to a TOF of 9.8 × 10^3 s^{-1}. The comparison of these performances with others reported in the literature is not easy because the supports are often crystalline and/or silica might be present but not considered, as pointed out in the introduction section.

For instance, to study the hydrogen productivity in MSR in relation to the amount of copper and its oxidation states, Oguchi et al. [28] had prepared a series of copper-based catalysts supported on amorphous zirconia with different metal loadings. The catalyst with 10 wt.% of copper exhibited a double hydrogen productivity than ours. They had used a classical precipitation technique at pH of 11. Even when low pH values were used, such as in the case of the work by Yao et al. [18] with an oxalate gel-coprecipitation method, the comparison is hard to make. In their work the final catalysts featured a Cu/Zr molar ratio of 4, whereas in the catalysts here studied the Cu/Zr ratio is always about 0.25 (mol/mol). That being said, the few catalysts prepared at comparable conditions on pure zirconia [18,28] are reported as more active than ours which further supports our hypothesis on the beneficial role of silica.

Indeed, by adding a low amount of silica into the support, that is Cu/ZrSi3, both the methanol conversion and the hydrogen productivity considerably increase to 55% and 284 mmol h^{-1} $g_{cat}{}^{-1}$, which correspond to enhancement factors of about 2.5 and 3.2, respectively. More interestingly, the addition of few silica promotes the hydrogen selectivity, with the H_2/CO_2 molar ratio going from 2.35 with the Cu/Zr catalyst to 2.91 with Cu/ZrSi3.

With the Cu/ZrSi10 catalyst both the conversion and the hydrogen productivity further rise to 73% and 370 mmol h^{-1} $g_{cat}{}^{-1}$, corresponding to enhancement factors of 3.7 and 4.1 over the Cu/Zr catalyst,

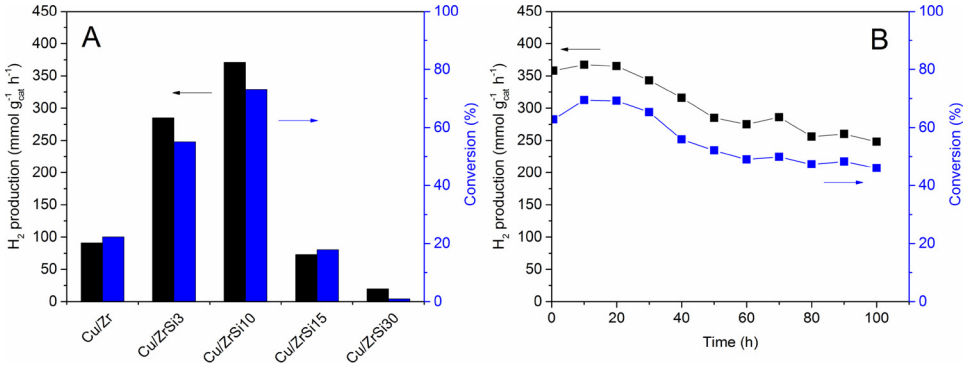

Fig. 4. Methanol steam reforming hydrogen production rate (black) and conversion (blue) after 20 h of reaction (A), and long term stability test with Cu/ZrSi10 (B). Reaction conditions: 260 °C, S/C = 1.3, and GHSV = 3500 h^{-1} (For interpretation of the references to colour in this figure legend, the reader is referred to the web version of this article).

respectively. The TOF increases as well to 23.4 × 10^3 s^{-1}. The hydrogen selectivity remains high, featuring a 2.94 H_2/CO_2 ratio, and the CO is always negligible. This catalyst showed stable catalytic activity, especially within 30 h time-on-stream, then a decrease was observed. To note that the test was performed under harsh conditions due to the high space velocity (GHSV of 3500 h^{-1}).

Interestingly, the increase over the Cu/ZrSi3 catalyst activity is purely due to the higher surface area of Cu/ZrSi10. As displayed in Figure S11, if the hydrogen productivity is normalized over the surface area of the catalysts, the Cu/ZrSi3 and Cu/ZrSi10 catalysts exhibit practically the same value around 1.5 mmol h^{-1} m_{cat}^{-2}. And that is not so unexpected as their morphological and reducibility features are almost identical.

From the data reported by Agrell et al. [69] and Ribeirinha [70] on the activity of a commercial benchmark system, that is the Cu/ZnO/Al_2O_3 catalyst by Süd-Chemie (G-66 MR), some considerations can be drawn on our Cu/ZrSi10 catalyst. At comparable experimental conditions, meaning similar total Cu content in the reactor, S/C ratio, space velocity, and reaction temperature, the two catalysts exhibit a very similar methanol conversion of about 70% and negligible CO production. However, the hydrogen productivity of G-66 MR is markedly lower than that of our catalyst (60 vol.% vs 75 vol.% of hydrogen in the outlet, respectively). Moreover, the commercial catalyst shows signs of deactivation right after few hours on stream, whereas ours is stable for 30 h.

As the silica content into the support raises to 15 wt.%, the catalytic performances drop until the almost zero activity of the Cu/ZrSi30 catalyst. Both the conversion and the hydrogen productivity are suppressed, along with the hydrogen selectivity showing a H_2/CO_2 ratio of 2.31. The selectivities to CH_4 and CO remain close to zero.

Since the surface areas of both Cu/ZrSi15 and Cu/ZrSi30 are much higher than those of the Cu/Zr and Cu/ZrSi10 catalysts (see Table 1), and the copper particles are still below 10 nm, the reason of such a dramatic decrease in activity might be due to a different surface chemistry of the support and/or different electronics of the copper nanoparticles.

To gain a more detailed understanding of the addition of silica on the reactivity, catalytic tests at different temperatures were carried out. Fig. 5 presents the catalytic performances between 100 °C and 300 °C, along with the Arrhenius plots (ln r vs 1/T, where r is the hydrogen productivity expressed as moles of hydrogen per second per gram of catalyst).

It is evident that Cu/ZrSi10 outperforms the other two catalysts at all temperatures. In particular, to display a methanol conversion level around 20%, the Cu/Zr catalyst needs about 60 °C more than Cu/ZrSi10.

The E_a calculated from the slopes of the Arrhenius plots are similar for the Cu/Zr and Cu/ZrSi30 catalysts with values of 81.5 kJ mol^{-1} and 91.1 kJ mol^{-1}, respectively. On the other hand, Cu/ZrSi10 exhibits a considerably lower value of 54.9 kJ mol^{-1}, meaning that the addition of a relatively small amount of silica significantly alters the catalytic active center. Although a meaningful comparison between apparent E_a values of MSR determined in different works is hard to make due to its the dependence on many parameters, such as the very catalyst and the experimental conditions, some values can be found with copper catalysts supported on zirconia or other oxides [32,70,71].

The one here found for the Cu/Zr catalyst is basically in line with those reported for similar systems, while that of Cu/ZrSi10 is markedly lower. For example, Mastalir et al. [32] calculated the apparent E_a values of a series of Cu/ZrO_2-CeO_2 catalysts with different copper loadings. They determined a tight correlation between exposed surface copper and the apparent E_a thus explaining the high copper loadings typical of catalysts for MSR [18,20,46,47]. For their catalyst at 12 wt.% of Cu loading, they reported an apparent E_a value of 85.4 kJ mol^{-1}, which is practically the same of the Cu/Zr catalyst herein studied. As the copper loading–and in turn the total copper exposed per gram of catalyst–increased to 35 wt.%, the apparent E_a decreases to about 60 kJ mol^{-1}.

As to this work, the higher performances of the Cu/ZrSi10 catalyst can surely be ascribable to the higher copper dispersion. But the lower activation energy (54.9 vs 81.5 kJ mol^{-1}) and the higher TOF (23.4 × 10^3 vs 9.8 × 10^3 s^{-1}) than the Cu/Zr catalyst indicate that some significant alteration of the active site occurred with the addition of silica for the benefit of the hydrogen production.

In order to gain some insights on the different reactivity and to elucidate the so different catalytic performances shown by the catalysts, FTIR experiments were carried out by treating the reduced catalysts with water vapors at the reaction temperature (260 °C) followed by methanol adsorption at room temperature. The spectrum of the catalysts before the contact of the methanol was used as background. Fig. 6 shows the spectra of the catalysts collected after degassing at room temperature and at 200 °C. At this temperature the reaction intermediates can be better appreciated, while for a complete overview of all the desorption spectra the reader is referred to Figure S12.

The purpose of Figure S13 is to show the variation of the surface −OH in the range 3000-3750 cm^{-1} normalized against the spectrum collected at 100 °C as the spectrum at room temperature might be

Table 3
Conversion, hydrogen productivity, H_2/CO_2 ratio, TOF, and apparent E_a after 20 h of reaction (260 °C, S/C = 1.3, GHSV = 3500 h^{-1}).

Entry	Conversion (%)	H_2 production (mmol g_{cat}^{-1} h^{-1})	H_2/CO_2 (mol/mol)	TOF ($10^3 s^{-1}$)	Ea (kJ mol^{-1})
Cu/Zr	20	91	2.35	9.8	81.5
Cu/ZrSi10	73	370	2.94	23.4	54.9
Cu/ZrSi30	2	38	2.31	–	91.1

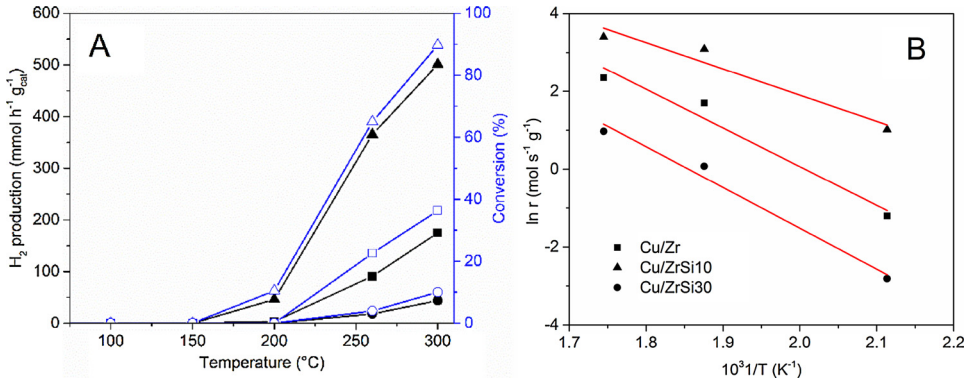

Fig. 5. Hydrogen productivity (solid marks) and methanol conversion (empty marks) during MSR reactions of Cu/Zr, Cu/ZrSi10, and Cu/ZrSi30 catalysts (A), and the corresponding Arrhenius plots (B).

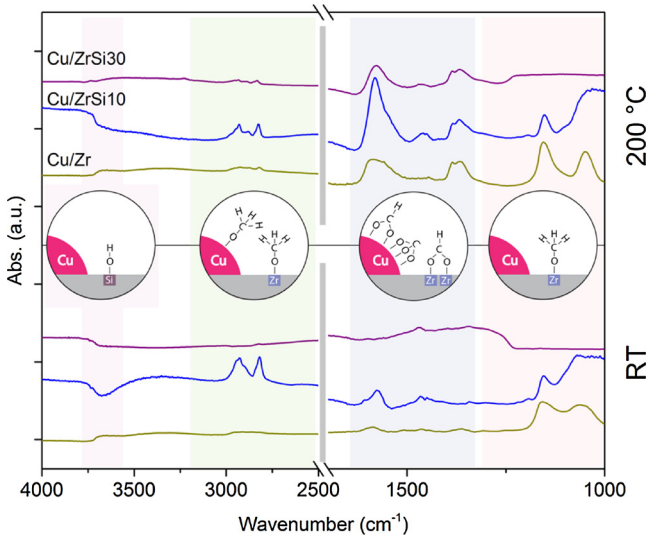

Fig. 6. FTIR methanol desorption spectra of Cu/Zr, Cu/ZrSi10, and Cu/ZrSi30 catalysts collected at room temperature (low) and at 200 °C (up).

altered by the methanol adsorption [13,40–42].

At room temperature, two bands at 1155 cm^{-1} and 1048 cm^{-1}, due to the stretching of C–O bonds, are immediately visible in the spectrum of the Cu/Zr catalyst. Bell an co-workers [13,40–42] assigned these bands to methoxy species adsorbed on zirconium sites (CH_3O-Zr). However, many of the other reaction intermediates contain C–O bonds, especially methoxy adsorbed on copper (CH_3O-Cu). So, any consumption of the CH_3O-Zr species must be deduced from more peculiar bands, like those due to the stretching of the C–H bonds at 2930 cm^{-1} [13,40–42].

In the spectra of the other catalysts the region between 800 cm^{-1} and 1200 cm^{-1} is progressively obscured by the presence of silica into the support [62] until no bands due to the C–O stretching are visible in the Cu/ZrSi30 catalysts. Nonetheless, in the Cu/ZrSi10 the band at 1155 cm^{-1} is still resolved so it is safe to assume that in all the silica-containing catalysts the methanol adsorbs forming methoxy species.

In parallel with methanol adsorption, in the spectrum of Cu/Zr catalyst, the overall intensity of −OH region increases, meaning that methanol adsorbs preferentially on the zirconium sites with the consequent formation of more surface −OH groups [72]. On the contrary, and very interestingly, in the Cu/ZrSi10 catalyst the methanol adsorbs prevalently on the copper (CH_3O-Cu), as revealed by the peculiar bands at 2926, 2988, 2814 cm^{-1} [13,40–42]. The only alteration of the −OH region is a marked decrease at 3676 cm^{-1} ascribable to −OH groups on silica (HO-Si) [13,40–42]. This indicates that the adsorption of methanol is followed by the consumption of surface −OH groups to form bidentate formates on zirconium sites (b-HCOO-Zr) that feature a pair of bands at 1580 cm^{-1} and 1386 cm^{-1} [13,40–42].

Their presence at room temperature means that not only the copper is the preferential adsorption site in Cu/ZrSi10, but also that it can effectively dehydrogenate the methoxy species. In the other catalysts almost no intermediates adsorbed on copper were detected.

In addition, carbonates adsorbed on copper (CO_3-Cu) were detected in this sample, as evidenced by the bands located between 1450 cm^{-1} and 1470 cm^{-1} [13,40–42]. Since their intensity increases with the temperature (Figure S12), their origin might be the direct decomposition of the b-HCOO species.

At 200 °C, bands associated to b-HCOO-Zr and b-HCOO-Cu (1560 and 1363 cm^{-1} [13,40–42] appear also in Cu/Zr and Cu/ZrSi10 catalysts, a clear indication of the dehydrogenation of the methoxy species. But in the Cu/ZrSi10 catalyst the intensity of the bands due to b-HCOO-Zr species is sensitively higher, roughly 2.8 times. Furthermore, with increasing the temperature, the CH_3O-Cu species constantly decrease (Figure S12) along with a marked −OH groups consumption (see Figure S13), while the Cu/Zr catalyst achieves a comparable consumption only at 300 °C and Cu/ZrSi30 does not show any at all (Figure S12).

And in this last catalyst the predominant formate species is the monodentate adsorbed on Cu (m-HCOO-Cu) (1572 and 1364 cm^{-1}) [13,40–42]. The persistence up to 260 °C of the reaction intermediates and surface −OH groups (Figure S12 and S13) indicates that the MSR activity is strongly inhibited. The little conversion observed at 300 °C is ascribable more to methanol decomposition rather than actual steam reforming, as also suggested by the H_2/CO_2 molar ratio of 2.31 of the outlet stream. These findings are consistent with other studies on MSR [1] and decomposition reactions [14] in which it was reported that the latter is more favored over Cu/SiO_2 catalysts. In the few works on MSR with copper catalysts supported on silica-based oxides, e.g. those by Deshmane et al. [62] and Yang et al. [73], S/C ratios as high as 10 had been used in order to push up the hydrogen production, whereas in this study the S/C was set to 1.3 (mol/mol).

These FTIR investigations revealed that the three catalysts feature completely different surface reactivities. The different adsorption site of the methanol is reasonably the key of the improved activity of Cu/ZrSi10 as the hydrogen extraction from the methoxy species is considered to be the toughest of the reaction steps [74]. The dehydrogenation of the methoxy species formed directly onto the surface of the copper nanoparticles of Cu/ZrSi10 appears to be easier. This can be deduced by the constant decrease of the bands due to CH_3O-Cu species from room temperature until their total disappearance, whereas those ascribed to CH_3O-Zr species still persist even at 300 °C.

Typically, on a purely zirconia support, methanol adsorbs on the most electron poor site, that is zirconium [13,40–42,72]. The reason why the methanol preferentially adsorbs on copper and reacts so easily

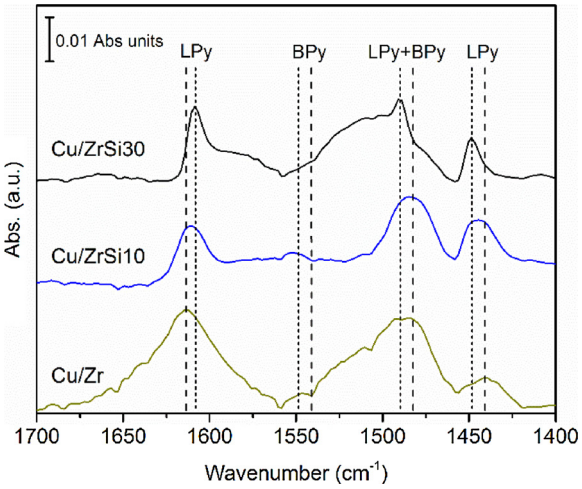

Fig. 7. FTIR-Py desorption spectra of Cu/Zr, Cu/ZrSi10, and Cu/ZrSi30 after degassing at 260 °C.

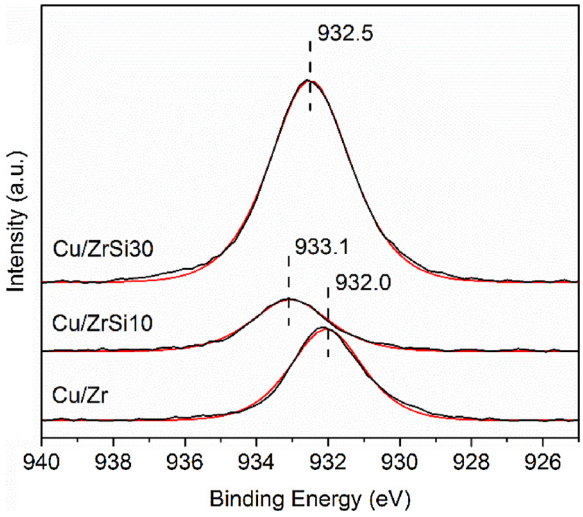

Fig. 8. Cu $2p_{3/2}$ XPS spectra of Cu/Zr, Cu/ZrSi10, and Cu/ZrSi30 catalysts after reduction.

in the Cu/ZrSi10 catalyst might be therefore due to a particularly high unsaturation of the copper nanoparticles.

Two complementary techniques were used to assess the presence and the extent of the surface unsaturation of the catalysts. First, we used the classical FTIR-pyridine desorption technique.

Fig. 7 shows the FTIR pyridine desorption spectra of Cu/Zr, Cu/ZrSi10, and Cu/ZrSi30 catalysts collected after reduction and degassing of the pyridine at the reaction temperature of 260 °C. The amount of the acid sites is reported per square meter of catalyst because of the different surface areas of the catalysts.

Lewis-type acid sites are predominant in the Cu/Zr catalyst with 0.10 μmol m^{-2}, as evidenced by the band centered around 1440-1448 cm^{-1}, with just a small amount of Brønsted acid sites (0.02 μmol m^{-2}) identified by the tiny band at around 1540-1550 cm^{-1} [9,75]. The amount of Lewis acid sites increases to 0.18 μmol m^{-2} in the Cu/ZrSi10 catalyst, while the Brønsted sites remain unchanged with 0.03 μmol m^{-2}. The Cu/ZrSi30 catalyst shows unaltered Lewis acid sites concentration compared to the Cu/Zr catalyst with 0.11 μmol m^{-2}, but no Brønsted acidity.

The surge in Lewis acidity (+80% over Cu/Zr and Cu/ZrSi30 catalysts) demonstrates that in the Cu/ZrSi10 catalyst the surface unsaturation is considerably higher than in the others. The previous speculation on the different adsorption site of methanol in Cu/ZrSi10 hence finds support in this much higher presence of Lewis acid centers [5–7].

However, FTIR spectroscopic analyses cannot identify the origin of the acidity but simply tell which acid sites are present and in what quantity. We can surmise that a direct influence of silica on the overall acidity is unlikely since there is no linear correlation between the acidity and the content of silica in our catalysts. This does not mean that the support and/or the silica have no influence at all.

To better understand the source of such Lewis acidity, the catalysts surfaces were studied by XPS analysis before and after the reduction treatment at 270 °C in hydrogen.

The spectra of the Cu $2p_{3/2}$ region between 925 eV and 940 eV are shown in Fig. 8, while that between 925 eV and 970 eV along with the Auger spectra are reported in Figures S14-16. Those of O 1s, Zr $3d_{5/2}$, and Si 2p can be found in Figure S17, S18, and S19, respectively.

The position of the Si 2p peak remains identical, irrespective of the silica content and the reduction treatment, and for this reason it was used for the charge compensation in the silica-containing catalysts.

Useful insights on the supports can be gained from the O 1s spectra. Values of binding energy (BE) of the O 1s peak near 530.5 eV are typical of M−O−M bonds, while values around 532.0 eV are associated to hydroxyl groups or oxo-hydroxo networks [64,76]. In the Cu/Zr catalyst, the O 1s peak is centered at 530.6 eV after the reduction. This value is in good accordance with the crystalline zirconia revealed by the XRPD analyses. As the silica content increases, the O 1s peak position shifts to higher BE, up to 531.8 eV in Cu/ZrSi30. This suggests the that the support consists of an amorphous oxo-hydroxylated zirconia [77], once again in accordance with the XRPD data. Bosman et al. [78] reported a similar trend but assigned the different positions of the O 1s peak to the proximity of oxygen to either Zr or Si. Specifically, they associated higher BE values to O near Si, indicating a depletion of the electron density and a consequent loss of the basic power.

The Zr $3d_{5/2}$ peak of the Cu/Zr catalyst falls at 182.8 eV, a value generally reported for pure zirconia supports and indicates the presence of Zr^{4+} cations [76]. In both Cu/ZrSi10 and Cu/ZrSi30 the Zr cations have lower electron density as evidenced by the Zr $3d_{5/2}$ peaks shift to 183.4 eV and 183.6 eV, respectively [31]. The absence in all catalysts before and after the reduction of a lower BE peak at around 180.8 eV indicates that even in the purely zirconia-supported catalysts there are no oxygen vacancies [34]. Furthermore, from the BE values obtained here for the Zr $3d_{5/2}$ and O 1s peaks, it can be deduced that no copper is incorporated into the lattice of the support [34]. The incipient wetness impregnation used for the preparation of all the catalysts seems to have prevented any loss of copper, which also explains the generally high copper exposures of these catalysts.

As expected, the copper is in the Cu^{2+} oxidation state in all the as-synthesized catalysts with the Cu $2p_{3/2}$ peak being always around BE of 935.0 eV [11] (Table 4). After the reduction, the shake-up peaks disappear, meaning that the surface is composed only of Cu^0 and/or Cu^+ [11]. The XRPD analyses evidenced that although the formation of some Cu^+-containing phase occurs during the reduction treatment in both the silica-containing catalysts, only metallic copper reflections are observed after the reduction (along with just a minor residual of CuO phase in Cu/ZrSi30). Such findings are in good accordance with the Auger parameter values (Table 3) that approach 1851.0 eV for all the

Table 4
Binding energies of the Cu $2p_{3/2}$ peak, Auger parameter (α'), and Cu/Zr ratios of all catalysts.

	BE Cu $2p_{3/2}$ (eV)			Cu/Zr	
Entry	Not reduced	Reduced	α' (eV)	Not reduced	Reduced
Cu/Zr	934.8	932.0	1851.1	0.12	0.07
Cu/ZrSi10	935.6	933.1	1851.0	0.20	0.06
Cu/ZrSi30	935.2	932.5	1851.3	0.23	0.32

reduced samples meaning that only metallic copper exists on the surface of the catalysts after the reduction [11].

Interestingly, the Cu $2p_{3/2}$ peak position after the reduction of the Cu/ZrSi10 falls at 933.1 eV, a sensitively higher BE value than in the other catalysts (Fig. 8 and Table 4) and in the copper-based catalysts reported in the literature [11,17,18,79,80]. This peak at such high BE implies that the surface of the copper nanoparticles in Cu/ZrSi10 is highly electron deficient, whereas those of the other catalysts are much richer in electrons.

The very same value was reported by Espinós et al. [81] for metallic copper deposited on a zirconium foil at surface Cu/Zr coverage ratio of 0.1. This observation fits quite well with the Cu/Zr ratio of 0.06 of the Cu/ZrSi10 catalyst after the reduction (Table 3). Even when the presence of Cu^+ sites had been clearly revealed, like in the case of the work of Samson et al. [11], the Cu $2p_{3/2}$ peak was only at 932.7 eV.

In spite of the higher silica content, which could have further depleted the electron density from the copper as it does with zirconium, the Cu $2p_{3/2}$ peak position in Cu/ZrSi30 does not reach the value of Cu/ZrSi10 and is falls at 932.5 eV. The reason is likely that Cu/ZrSi30 suffers from a lower metal-support interaction, as evidenced by the H_2-TPR analyses, and a generally lower stability of the nanoparticles, in part ascribable to the larger pores (Table 1). The result is a surface accumulation of copper (Cu/Zr surface ratio of 0.32 after the reduction) in the form of bigger nanoparticles (6–7 nm) whose surface is more negatively charged and resembles that of bulkier copper [31,17,81]. The BE of 932.5 eV found for this catalyst perfectly matches with that reported by Espinós et al. [81] for a similar surface coverage, and with that of Sato et al. [82] for a copper catalyst prepared at elevated pH and supported on amorphous zirconia.

Some of us [60] found a somewhat unexpected Lewis acidity of metallic copper nanoparticles in the range of 2–4 nm. The surprisingly high activity of a Cu/SiO_2 catalyst, achieved without using any acidic support, was ascribed to particularly small copper nanoparticles exhibiting high Lewis acidity. Now, we have clarified that such acidity is not due to well-defined Cu^+ sites but rather to the particularly electron poor surface of the metallic copper nanoparticles.

The MSR reaction needs a prompt hydrogen extraction from the adsorbed intermediates, particularly from the methoxy species, which is promoted by Cu^+ sites, as well as extended metallic copper surface for the molecular hydrogen production [1]. In the Cu/ZrSi10 here studied, although Cu^+ sites were not observed after the reduction, the hydrogen productivity is about four times that of the silica-free catalyst. The reason is clearly the much higher presence of unsaturated sites.

The silica did not permit the formation of oxygen vacancies and dragged electron density away of Zr, O, and Cu. This would make the surface of the Cu/ZrSi30 catalyst the most unsaturated. In fact, it is the Cu/ZrSi10 catalyst that features the highest overall surface unsaturation. Since both Zr and O sites are more electron poor in Cu/ZrSi30, the source of the high surface unsaturation in Cu/ZrSi10 detected with the FTIR analyses is surely the copper.

Indeed, in this last catalyst, the surface of the copper nanoparticles was found much more electron poor than in the other ones, although the particles themselves are in the metallic state. The enhanced hydrogen productivity shown by Cu/ZrSi10 then finds explanation in the particularly electron poor surface of small copper nanoparticles (2–3 nm) on which the methanol preferentially adsorbs thus facilitating the overall reaction pathway [74].

Copper catalysts can be considered as bifunctional catalysts due to the presence of Cu^+ sites and the synergies between copper phases and the support [60,83]. With this work we have demonstrated that the very same bifunctionality can be achieved by tailoring the size of the nanoparticles without sacrificing any copper site to any specific role. In practice, thanks to the peculiar electronic structure of the copper nanoparticles, we were able to preferentially drive the reaction towards a much easier path, which takes place directly on the dehydrogenation sites. This *all-in-one* copper, along with its high exposure, has led to a catalyst that fulfills all the requirements of the MRS reaction but that, despite its simplicity and low copper content, shows a remarkable hydrogen productivity even when compared to some of the benchmark catalysts reported in the literature [1,21,32,35,69,70].

4. Conclusions

In this work, the electronic properties of copper nanoparticles were tuned to enhance the catalytic activity of a Cu/ZrO_2 catalyst in the MSR reaction. With this innovative approach, all the catalytic steps are performed by the copper, starting from the methanol adsorption and dissociation, until the dehydrogenation of the intermediates and the subsequent production of molecular hydrogen.

Such *all-in-one* copper site was generated by exploiting the different electronics of the surface of the nanoparticles when their size is in the range of 2–3 nm. In fact, although being in the metallic state, the surface of these so small nanoparticles was found highly unsaturated and electron poor, but no Cu^+ was detected.

The methanol adsorbs directly on the copper and then undergoes the dehydrogenation reactions typical of a formate-based pathway of the MSR reaction, while the metallic nature of the nanoparticles allows the production of molecular hydrogen on the very same site. The hydrogen productivity is four times higher than that of the silica-free catalyst and matches that of the best performing catalysts but featuring much higher copper loadings and doped with precious metals [1,21,32,35,69,70].

To produce such copper nanoparticles, a specific amount of silica (10 wt.%) was incorporated into the zirconia support via a sol-gel method. This support proved superior to a pure zirconia as it is amorphous and with narrower pores. More importantly, the presence of silica did not allow the copper to excessively grow during the reduction treatment thus leading to the previously described effects. For higher levels of silica (> 10 wt.% of the support) the material shows more silica-like characteristic that do not favor the MSR reaction and do not stabilize the copper against aggregation.

Declaration of Competing Interest

The authors declare that they have no known competing financial interests or personal relationships that could have appeared to influence the work reported in this paper.

Acknowledgements

This activity has received funding from the European Institute of Innovation and Technology (EIT). This body of the European Union receives support from the European Union's Horizon 2020 research and innovation program. The authors acknowledge the Hugarian-Italian HAS-CNR bilateral project and ESRF for the provision of the beamtime.

Appendix A. Supplementary data

Supplementary material related to this article can be found, in the online version, at doi:https://doi.org/10.1016/j.apcatb.2019.118016.

References

[1] D. Li, X. Li, J. Gong, Catalytic reforming of oxygenates: state of the art and future prospects, Chem. Rev. 116 (2016) 11529–11653.
[2] C. Huck-Iriart, L. Soler, A. Casanovas, C. Marini, J. Prat, J. Llorca, C. Escudero, Unraveling the chemical state of cobalt in Co-based catalysts during ethanol steam reforming: an in situ study by near ambient pressure XPS and XANES, ACS Catal. 8 (2018) 9625–9636.
[3] D. Liu, Y. Men, J. Wang, G. Kolb, X. Liu, Y. Wang, Q. Sun, Highly active and durable $Pt/In_2O_3/Al_2O_3$ catalysts in methanol steam reforming, Int. J. Hydrogen Energy 4 (2016) 21990–21999.
[4] J. Károlyi, M. Németh, C. Evangelisti, G. Sáfrán, Z. Schay, A. Horváth, F. Somodi, Carbon dioxide reforming of methane over Ni–In/SiO_2 catalyst without coke

formation, J. Ind. Eng. Chem. 58 (2018) 189–201.
[5] F. Bossola, X. Pereira-Hernández, C. Evangelisti, Y. Wang, V. Dal Santo, Investigation of the promoting effect of Mn on a Pt/C catalyst for the steam and aqueous phase reforming of glycerol, J. Catal. 349 (2017) 75–83.
[6] Z. Wei, A. Karim, Y. Li, Y. Wang, Elucidation of the roles of Re in aqueous-phase reforming of glycerol over Pt−Re/C catalysts, ACS Catal. 5 (2015) 7312–7320.
[7] Z. Wei, A. Karim, Y. Li, D. King, Y. Wang, Elucidation of the roles of Re in steam reforming of glycerol over Pt–Re/C catalysts, J. Catal. 322 (2015) 49–59.
[8] A. Kirilin, A. Tokarev, H. Manyar, C. Hardacre, T. Salmi, J.-P. Mikkola, D. Murzin, Aqueous phase reforming of xylitol over Pt-Re bimetallic catalyst: effect of the Re addition, Cat. Today 223 (2014) 97–107.
[9] N. Scotti, F. Zaccheria, C. Evangelisti, R. Psaro, N. Ravasio, Dehydrogenative coupling promoted by copper catalysts: a way to optimise and upgrade bio-alcohols, Catal. Sci. Technol. 7 (2017) 1386–1393.
[10] S. Tada, A. Katagiri, K. Kiyota, T. Honma, H. Kamei, A. Nariyuki, S. Uchida, S. Satokawa, Cu species incorporated into amorphous ZrO_2 with high activity and selectivity in CO_2-to-methanol hydrogenation, J. Phys. Chem. C 122 (2018) 5430–5442.
[11] K. Samson, M. Śliwa, R. Socha, M. Gòra-Marek, D. Mucha, D. Rutkowska-Zbik, J.-F. Paul, M. Ruggiero-Mikołajczyk, R. Grabowski, J. Słoczyński, Influence of ZrO_2 structure and copper electronic state on activity of Cu/ZrO_2 catalysts in methanol synthesis from CO_2, ACS Catal. 4 (2014) 3730–3741.
[12] Y. Sun, L. Chen, Y. Bao, G. Wang, Y. Zhang, M. Fu, J. Wu, D. Ye, Roles of nitrogen species on nitrogen-doped CNTs supported Cu-ZrO_2 system for carbon dioxide hydrogenation to methanol, Catal. Today 307 (2018) 212–223.
[13] I. Fisher, A. Bell, A mechanistic study of methanol decomposition over Cu/SiO_2, ZrO_2/SiO_2, and Cu/ZrO_2/SiO_2, J. Catal. 184 (1999) 357–376.
[14] T. Tsoncheva, I. Genova, M. Dimitrov, E. Sarcadi-Priboczki, A. Venezia, D. Kovacheva, N. Scotti, V. Dal Santo, Nanostructured copper-zirconia composites as catalysts for methanol decomposition, Appl. Catal. B: Environ. 165 (2015) 599–610.
[15] G.-S. Wu, L.-C. Wang, Y.-M. Liu, Y. Cao, W.-L. Dai, H.-Y. He, K.-N. Fan, Implication of the role of oxygen anions and oxygen vacancies for methanol decomposition over zirconia supported copper catalysts, Appl. Surf. Sci. 253 (2006) 974–982.
[16] H. Purnama, F. Girgsdies, T. Ressler, J. Schattka, R. Caruso, R. Schomäcker, R. Schlögl, Activity and selectivity of a nanostructured CuO/ZrO_2 catalyst in the steam reforming of methanol, Catal. Letters 94 (2004) 61–68.
[17] I. Ritzkopf, S. Vukojević, C. Weidenthaler, J.-D. Grunwaldt, F. Schüth, Decreased CO production in methanol steam reforming over Cu/ZrO_2 catalysts prepared by the microemulsion technique, Appl. Catal. A Gen. 302 (2006) 215–223.
[18] C.-Z. Yao, L.-C. Wang, Y.-M. Liu, G.-S. Wu, Y. Cao, W.-L. Dai, H.-Y. He, K.-N. Fan, Effect of preparation method on the hydrogen production from methanol steam reforming over binary Cu/ZrO_2 catalysts, Appl. Catal. A Gen. 297 (2006) 151–158.
[19] S. Yong, C. Ooi, S. Chai, X. Wu, Review of methanol reforming-Cu-based catalysts, surface reaction mechanisms, and reaction schemes, Int. J. Hydrogen Energy 38 (2013) 9541–9552.
[20] J. Zhou, Y. Zhang, G. Wu, D. Mao, G. Lu, Influence of the component interaction over Cu/ZrO_2 catalysts induced with fractionated precipitation method on the catalytic performance for methanol steam reforming, RSC Adv. 6 (2016) 30176–30183.
[21] S. Sá, H. Silva, L. Brandão, J. Sousa, A. Mendes, Catalysts for methanol steam reforming—a review, Appl. Catal. B: Environ. 99 (2010) 43–57.
[22] S. Davidson, H. Zhang, J. Sun, Y. Wang, Supported metal catalysts for alcohol/sugar alcohol steam reforming, Dalton Trans. 43 (2014) 11782–11802.
[23] J. Papavasiliou, G. Avgouropoulos, T. Ioannides, Effect of dopants on the performance of CuO–CeO_2 catalysts in methanol steam reforming, Appl. Catal. B: Environ. 69 (2007) 226–234.
[24] M. Turco, G. Bagnasco, C. Cammarano, P. Senese, U. Costantino, M. Sisani, Cu/ZnO/Al_2O_3 catalysts for oxidative steam reforming of methanol: the role of Cu and the dispersing oxide matrix, Appl. Catal. B: Environ. 77 (2007) 46–57.
[25] Y. Matsumura, H. Ishibe, High temperature steam reforming of methanol over Cu/ZnO/ZrO_2 catalysts, Appl. Catal. B: Environ. 91 (2009) 524–532.
[26] H. Yang, Y. Chen, X. Cui, G. Wang, Y. Cen, T. Deng, W. Yan, J. Gao, S. Zhu, U. Olsbye, J. Wang, W. Fan, A highly stable copper-based catalyst for clarifying the catalytic roles of Cu^0 and Cu^+ species in methanol dehydrogenation, Angew. Chem. Int. Ed. 57 (2018) 1836–1840.
[27] L. Mayr, B. Klötzer, D. Zemlyanov, S. Penner, Steering of methanol reforming selectivity by zirconia–copper interaction, J. Catal. 321 (2015) 123–132.
[28] H. Oguchi, H. Kanai, K. Utani, Y. Matsumura, S. Imamura, Cu_2O as active species in the steam reforming of methanol by CuO/ZrO_2 catalysts, Appl. Catal. A Gen. 293 (2005) 64–70.
[29] J. Baneshi, M. Haghighi, N. Jodeiri, M. Abdollahifar, H. Ajamein, Homogeneous precipitation synthesis of CuO–ZrO_2–CeO_2–Al_2O_3 nanocatalyst used in hydrogen production via methanol steam reforming for fuel cell applications, Energy Convers. Manage. 87 (2014) 928–937.
[30] A. Lytkina, N. Orekhova, M. Ermilova, A. Yaroslavtsev, The influence of the support composition and structure ($M_xZr_{1-x}O_{2-d}$) of bimetallic catalysts on the activity in methanol steam reforming, Int. J. Hydrogen Energy 43 (2018) 198–207.
[31] L.-C. Wang, Q. Liu, M. Chen, Y.-M. Liu, Y. Cao, H.-Y. He, K.-N. Fan, Structural evolution and catalytic properties of nanostructured Cu/ZrO_2 catalysts prepared by oxalate gel-coprecipitation technique, J. Phys. Chem. C 111 (2007) 16549–16557.
[32] A. Mastalir, B. Frank, A. Szizybalski, H. Soerijanto, A. Deshpande, M. Niederberger, R. Schomäcker, R. Schlögl, T. Ressler, Steam reforming of methanol over Cu/ZrO_2/CeO_2 catalysts: a kinetic study, J. Catal. 230 (2005) 464–475.
[33] L.-C. Wang, Q. Liu, M. Chen, Y.-M. Liu, Y. Cao, H.-Y. He, K.-N. Fan, Structural evolution and catalytic properties of nanostructured Cu/ZrO_2 catalysts prepared by oxalate gel-coprecipitation technique, J. Phys. Chem. C 111 (2007) 16549–16557.
[34] V. Pakharukova, E. Moroz, V. Kriventsov, T. Larina, A. Boronin, L. Dolgikh, P. Strizhak, Structure and state of copper oxide species supported on yttria-stabilized zirconia, J. Phys. Chem. C 113 (2009) 21368–21375.
[35] A. Kubacka, M. Fernández-García, A. Martínez-Arias, Catalytic hydrogen production through WGS or steam reforming of alcohols over Cu, Ni and Co catalysts, Appl. Catal. A Gen. 518 (2016) 2–17.
[36] Y. Li, X. Dong, W. Lin, Effects of ZrO_2-promoter on catalytic performance of CuZnAlO catalysts for production of hydrogen by steam reforming of methanol, Int. J. Hydrogen Energy 29 (2004) 1617–1621.
[37] J. Kirkland, M. van Straten, H. Claessens, High pH mobile phase effects on silica-based reversed-phase high-performance liquid chromatographic columns, J. Chromatogr. 691 (1995) 3–19.
[38] D. Wolff-Boenisch, S. Gislason, E. Oelkers, C. Putnis, The dissolution rates of natural glasses as a function of their composition at pH 4 and 10.6, and temperatures from 25 to 74 °C, Geochim. Acta 68 (2004) 4843–4858.
[39] Q. Zhao, W.-H. Shih, H.-L. Chang, P. Andersen, The effect of curing on the thermal stability of Si-doped ZrO_2 powders, Appl. Catal. A Gen. 262 (2004) 215–221.
[40] I. Fisher, H. Woo, A. Bell, Effects of zirconia promotion on the activity of Cu/SiO_2 for methanol synthesis from CO/H_2 and CO_2/H_2, Catal. Letters 44 (1997) 11–17.
[41] I. Fisher, A. Bell, In-situ infrared study of methanol synthesis from H_2/CO_2 over Cu/SiO_2 and Cu/ZrO_2/SiO_2, J. Catal. 172 (1997) 222–237.
[42] I. Fisher, A. Bell, In situ infrared study of methanol synthesis from H_2/CO over Cu/SiO_2 and Cu/ZrO_2/SiO_2, J. Catal. 178 (1998) 153–173.
[43] D. Bianchi, T. Chafik, M. Khalfallah, S. Teichner, Intermediate species on zirconia supported methanol aerogel catalysts - V. Adsorption of methanol, Appl. Catal. A Gen. 123 (1995) 89–110.
[44] F. Zaccheria, N. Scotti, M. Marelli, R. Psaro, N. Ravasio, Unravelling the properties of supported copper oxide: can the particle size induce acidic behaviour? Dalton Trans. 42 (2013) 1319–1328.
[45] N. Shamsul, S. Kamarudin, N. Rahman, N. Kofli, An overview on the production of bio-methanol as potential renewable energy, Ren. Sust. Energy Rev. 33 (2014) 578–588.
[46] G. Huang, B.-J. Liaw, C.-J. Jhang, Y.-Z. Chen, Steam reforming of methanol over CuO/ZnO/CeO_2/ZrO_2/Al_2O_3 catalysts, Appl. Catal. A Gen. 358 (2009) 7–12.
[47] P. Clancy, J. Breen, J. Ross, The preparation and properties of coprecipitated Cu–Zr–Y and Cu–Zr–La catalysts used for the steam reforming of methanol, Catal. Today 127 (2007) 291–294.
[48] D. Das, J. Llorca, M. Dominguez, S. Colussi, A. Trovarelli, A. Gayen, Methanol steam reforming behavior of copper impregnated over CeO_2-ZrO_2 derived from a surfactant assisted coprecipitation route, Int. J. Hydrogen Energy 40 (2015) 10463–10479.
[49] C. Mateos-Pedrero, H. Silva, D. Pacheco Tanaka, S. Liguori, A. Iulianelli, A. Basile, A. Mendes, CuO/ZnO catalysts for methanol steam reforming: the role of the support polarity ratio and surface area, Appl. Catal. B: Environ. 174-175 (2015) 67–76.
[50] Z.-Q. Wang, Z.-N. Xu, S.-Y. Peng, M.-J. Zhang, G. Lu, Q.-S. Chen, Y. Chen, G.-C. Guo, High-performance and long-lived Cu/SiO_2 nanocatalyst for CO_2 hydrogenation, ACS Catal. 5 (2015) 4255–4259.
[51] Z. Yuana, L. Wang, J. Wang, S. Xia, P. Chen, Z. Hou, X. Zheng, Hydrogenolysis of glycerol over homogenously dispersed copper on solid base catalysts, Appl. Catal. B: Environ. 101 (2011) 431–440.
[52] A. Hill, A new gas system for automated in situ powder diffraction studies at the European Synchrotron Radiation Facility, J. Appl. Cryst. 46 (2013) 570–572.
[53] G. Ashiotis, A. Deschildre, Z. Nawaz, J. Wright, D. Karkoulis, F. Picca, J. Kieffer, The fast azimuthal integration Python library: pyFAI, J. Appl. Cryst. 48 (2015) 510–519.
[54] A. Altomare, N. Corriero, C. Cuocci, A. Falcicchio, A. Moliterni, R. Rizzi, QUALX2.0: a qualitative phase analysis software using the freely available database POW_COD, J. Appl. Cryst. 48 (2015) 598–603.
[55] A. Larson, R. Von Dreele, General Structure Analysis System (GSAS), Los Alamos National Laboratory Report LAUR, Los Alamos, 2004.
[56] A. Gallo, C. Pirovano, P. Ferrini, M. Marelli, R. Psaro, S. Santangelo, G. Faggio, V. Dal Santo, Influence of reaction parameters on the activity of ruthenium based catalysts for glycerol steam reforming, Appl. Catal. B: Environ. 121–122 (2012) 40–49.
[57] G. Williamson, W. Hall, X-ray line broadening from filed aluminium and wolfram, Acta Mater. 1 (1953) 22–31.
[58] Y. Matsumura, H. Ishibe, Suppression of CO by-production in steam reforming of methanol by addition of zinc oxide to silica-supported copper catalyst, J. Catal. 268 (2009) 282–289.
[59] X. Zhang, L. Wang, Y. Cao, W. Dai, H. He, K. Fan, Unique microwave effect on the microstructural modification of Cu/ZnO/Al_2O_3 catalysts for steam reforming of methanol, Chem. Comm. (2005) 4104–4106.
[60] N. Scotti, M. Dangate, A. Gervasini, C. Evangelisti, N. Ravasio, F. Zaccheria, Unraveling the role of low coordination sites in a Cu metal nanoparticle: a step toward the selective synthesis of second generation biofuels, ACS Catal. 4 (2014) 2818–2826.
[61] L. Balogh, G. Ribárik, T. Ungár, Stacking faults and twin boundaries in fcc crystals determined by x-ray diffraction profile analysis, J. Appl. Phys. 100 (2006).
[62] V. Deshmane, R. Abrokwah, D. Kuila, Synthesis of stable Cu-MCM-41 nanocatalysts for H_2 production with high selectivity via steam reforming of methanol, Int. J. Hydrogen Energy 40 (2015) 10439–10452.
[63] J. Słoczynski, R. Grabowski, A. Kozłowska, P. Olszewski, J. Stoch, Reduction kinetics of CuO in CuO/ZnO/ZrO_2 systems, Phys. Chem. Chem. Phys. 5 (2012) 4631–4640.
[64] G.-S. Wu, D.-S. Mao, G.-Z. Lu, Y. Cao, K.-N. Fan, The role of the promoters in Cu based catalysts for methanol steam reforming, Catal. Lett. 130 (2009) 177–184.

[65] T. Witoon, J. Chalorngtham, P. Dumrongbunditkul, M. Chareonpanich, J. Limtrakul, CO_2 hydrogenation to methanol over Cu/ZrO_2 catalysts: Effects of zirconia phases, Chem. Eng. J. 293 (2016) 327–336.
[66] Z. Liu, M. Amiridis, Y. Chen, Characterization of CuO supported on tetragonal ZrO_2 catalysts for N_2O decomposition to N_2, J. Phys. Chem. B 109 (2005) 1251–1255.
[67] J. Liu, J. Shi, D. He, Q. Zhang, X. Wu, Y. Liang, Q. Zhu, Surface active structure of ultra-fine Cu/ZrO_2 catalysts used for the CO_2 + H_2 to methanol reaction, Appl. Catal. A Gen. 218 (2001) 113–119.
[68] L. Kundakovic, M. Flytzani-Stephanopoulos, Cu- and Ag-modified cerium oxide catalysts for methane oxidation, J. Catal. 179 (1998) 203–221.
[69] J. Agrell, H. Birgersson, M. Boutonnet, Steam reforming of methanol over a Cu/ZnO/Al_2O_3 catalyst: a kinetic analysis and strategies for suppression of CO formation, J. Power Source 106 (2002) 249–257.
[70] P. Ribeirinha, C. Mateos-Pedrero, M. Boaventura, J. Sousa, A. Mendesa, CuO/ZnO/Ga_2O_3 catalyst for low temperature MSR reaction: synthesis, characterization and kinetic model, Appl. Catal. B: Environ. 221 (2018) 371–379.
[71] H. Purnama, T. Ressler, R. Jentoft, H. Soerijanto, R. Schlögl, R. Schomäcker, CO formation/selectivity for steam reforming of methanol with a commercial CuO/ZnO/Al_2O_3 catalyst, Appl. Catal. A Gen. 259 (2004) 83–94.
[72] P. Lustemberg, M. Bosco, A. Bonivardi, H. Busnengo, M. Ganduglia-Pirovano, Insights into the nature of formate species in the decomposition and reaction of methanol over cerium oxide surfaces: a combined infrared spectroscopy and density functional theory study, J. Phys. Chem. C 119 (2015) 21452–21464.
[73] R.-X. Yang, K.-H. Chuang, M.-Y. Wey, Hydrogen production through methanol steam reforming: effect of synthesis parameters on Ni-Cu/CaO-SiO_2 catalysts activity, Int. J. Hydrogen Energy 39 (2014) 19494–19501.
[74] B. Frank, F. Jentoft, H. Soerijanto, J. Krohnert, R. Schlogl, R. Schomacker, Steam reforming of methanol over copper-containing catalysts: influence of support material on microkinetics, J. Catal. 246 (2009) 177–192.
[75] J. Sun, R. Baylon, C. Liu, D. Mei, K. Martin, P. Venkitasubramanian, Y. Wang, Key roles of Lewis acid – base pairs on $Zn_xZr_yO_z$ in direct ethanol/acetone to isobutene conversion, J. Am. Chem. Soc. 138 (2016) 507–517.
[76] S. Basahel, M. Mokhtar, E. Alsharaeh, T. Ali, H. Mahmoud, K. Narasimharao, Physico-chemical and catalytic properties of mesoporous CuO-ZrO_2 catalysts, Catalysts 6 (2016) 57.
[77] J. Navío, M. Hidalgo, G. Colón, S. Botta, M. Litter, Preparation and physicochemical properties of ZrO_2 and Fe/ZrO_2 pepared by a sol-gel technique, Langmuir 17 (2001) 202–210.
[78] H. Bosman, A. Pijpers, A. Jaspers, An X-ray photoelectron spectroscopy study of the acidity of SiO_2–ZrO_2 mixed oxides, J. Catal. 161 (1996) 551–559.
[79] Y. Zhang, C. Ye, C. Guo, C. Gan, X. Tong, n2O3-modified Cu/SiO_2 as an active and stable catalyst for the hydrogenation of methyl acetate to ethanol, Chin. J. Catal. 39 (2018) 99–108.
[80] Z. Wang, W. Wang, G. Lu, Studies on the active species and on dispersion of Cu in Cu/SiO_2 and Cu/Zn/SiO_2 for hydrogen production via methanol partial oxidation, Int. J. Hydrogen Energy 28 (2003) 151–158.
[81] J. Espinós, J. Morales, A. Barranco, A. Caballero, J. Holgado, A. González-Elipe, Interface effects for Cu, CuO, and Cu_2O deposited on SiO_2 and ZrO_2. XPS determination of the valence state of copper in Cu/SiO_2 and Cu/ZrO_2 catalysts, J. Phys. Chem. B 106 (2002) 6921–6929.
[82] A. Sato, D. Volanti, D. Meira, S. Damyanova, E. Longo, J. Bueno, Effect of the ZrO_2 phase on the structure and behavior of supported Cu catalysts for ethanol conversion, J. Catal. 307 (2013) 1–17.
[83] A. Alba-Rubio, B. O'Neill, F. Shi, C. Akatay, C. Canlas, T. Li, R. Winans, J. Elam, E. Stach, P. Voyles, J. Dumesic, Pore structure and bifunctional catalyst activity of overlayers applied by atomic layer deposition on copper nanoparticles, ACS Catal. 4 (2014) 1554–1557.